Journal of Solid State Electrochemistry (2019) 23:1191–1199
https://doi.org/10.1007/s10008-019-04215-7

ORIGINAL PAPER

# Scalable one-pot synthesis of bismuth sulfide nanorods as an electrode active material for energy storage applications

**Agata Moyseowicz** [1]

Received: 6 December 2018 / Revised: 10 February 2019 / Accepted: 11 February 2019 / Published online: 19 February 2019


**Abstract**

The quest for developing the scalable methods of synthesis of materials with potential electrochemical energy storage applications remains a great challenge. Herein, we propose a facile, one-step chemical precipitation method for the synthesis of $Bi_2S_3$ with the nanorods morphology. Influence of different synthesis temperatures on the physical, chemical, and electrochemical performance was investigated. Relatively low BET surface area and mesopore volume of $Bi_2S_3$ increased with the higher reaction temperature. Bismuth sulfides synthesized at various temperatures were used as an electrode active material in supercapacitor. The semiconductive properties of $Bi_2S_3$ resulted in exceptional capacitive behavior. Bismuth sulfide synthesized at 75 °C exhibited a specific capacitance of 457 F $g^{-1}$ at 1 A $g^{-1}$ in 6 mol $L^{-1}$ KOH solution as an electrolyte. Moreover, material prepared at 75 °C maintained the best capacitance value at a large current density of 20 A $g^{-1}$, compared with bismuth sulfides synthesized at the temperatures of 0 °C and 25 °C.

**Keywords** Transition metal sulfide · Supercapacitor · Aqueous electrolyte

## Introduction

In the last decade, extensive efforts have been undertaken to develop new generation energy storage devices with high power and energy densities for the application in hybrid electric vehicles and portable electronics. Supercapacitors are considered as promising candidates for harvesting and delivering relatively high amount of energy in short periods of time, showing excellent reversibility and long life performance. Besides the carbon materials such as activated carbons, carbon nanofibers, or graphene oxides [1–8], transition metal compounds such as metal oxides or/and hydroxides are considered as attractive potential electrode materials for use in supercapacitors due to the high-capacitance values, which convert into the enhanced energy density [9–11]. Transition metal sulfides have been nowadays great candidates for use in hybrid supercapacitors due to their strong faradaic electrochemical response. Among various metal sulfides, nickel sulfide [12, 13], cobalt sulfide [14], nickel cobalt sulfide [15, 16], bismuth sulfide [17], and copper sulfide [18] have received considerable attention as an electrode active material with high pseudocapacitance for supercapacitors. Among aforementioned metal sulfides, $Bi_2S_3$ has drawn special attention due to the unique electric properties resulting from p-type semiconductor behavior with direct band gap ($Eg$) of ~ 1.3 eV [15]. These extraordinary features encourage further investigations of $Bi_2S_3$ in energy storage applications.

Several synthesis methods of nanosized bismuth sulfide have been reported, such as electrochemical deposition [19], sonochemical techniques [20], or microwave irradiation [21]. However, the most recently used method for $Bi_2S_3$ synthesis is hydrothermal (solvothermal) treatment [22, 23] which requires using thioacetamide, thiourea, L-cysteine, or sulfur sublimed at high temperature [24, 25]. Liang et al. [26] synthesized $Bi_2S_3$ in the nanorods form by the solvothermal method and used it as electrode-active material in supercapacitor, obtaining 270 F $g^{-1}$ at a current density of 1 A $g^{-1}$. The hierarchical $Bi_2S_3$ nanoflowers synthesized via hydrothermal method by Liu et al. [23] were characterized by the capacitance value of 233 F $g^{-1}$ at 1 A $g^{-1}$. In order to improve the

**Electronic supplementary material** The online version of this article (https://doi.org/10.1007/s10008-019-04215-7) contains supplementary material, which is available to authorized users.

✉ Agata Moyseowicz
agata.moyseowicz@pwr.edu.pl

[1] Department of Polymer and Carbonaceous Materials, Faculty of Chemistry, Wrocław University of Science and Technology, Gdańska 7/9, 50-344 Wrocław, Poland

supercapacitor performance, the $Bi_2S_3$ nanorods–graphene composite was synthesized by Vadivel et al. [24] resulting in a composite which exhibited a maximum specific capacitance of 290 F $g^{-1}$ at a current density of 1 A $g^{-1}$.

Compared with many other reported bismuth sulfide synthesis methods, which involve hydrothermal or solvothermal procedures, the proposed precipitation approach exhibits several advantages. The use of ammonium sulfide solution with a bismuth nitrate offers a cost-effective procedure for preparation of $Bi_2S_3$ nanostructures without use of sealed autoclaves and high synthesis temperatures. The proposed synthesis route stands out in terms of the synthesis time, which is several times faster compared with hydrothermal procedures and can be successfully applied in the larger scale without additional costs. Moreover, due to the simplified synthesis method, various modifications of the procedure parameters may be applied in order to adjust the electrochemical properties of bismuth sulfide nanostructures.

Herein, a facile chemical precipitation of bismuth sulfide as a novel approach for synthesis of $Bi_2S_3$ is proposed. We have evaluated the synthesis temperature as a factor influencing $Bi_2S_3$ physical and electrochemical properties. As-received bismuth sulfide nanorods were used as an active material of the electrode and exhibited a remarkable capacitance value of 457 F $g^{-1}$ at 1 A $g^{-1}$ when synthesized at 75 °C.

## Experiment

### Materials synthesis

Bismuth sulfides were synthesized using a facile chemical precipitation at 0, 25, and 75 °C. 1.9 mmol of bismuth nitrate ($Bi(NO_3)_3 \cdot 6H_2O$) was dissolved in distilled water. The solutions were adjusted to a set temperature (0, 25, and 75 °C) under vigorous mechanical stirring. Subsequently, the solution of ammonium sulfide ($(NH_4)_2S$) was added dropwise until precipitation of bismuth sulfide was complete. The resulting bismuth sulfides were washed several times with distilled water followed by centrifugation until the neutral pH of the solution is dried under a vacuum at 60 °C for 24 h.

### Characterization

The porous texture characteristics of the materials were determined by $N_2$ sorption at 77 K using a NOVA 2000 gas sorption analyzer (Quantachrome). Prior to measurements, the sample was outgassed overnight at 120 °C. The specific surface area ($S_{BET}$) was calculated from the Brunauer–Emmett–Teller (BET) equation. The amount of nitrogen adsorbed at a relative pressure of $p/p_0 = 0.96$ was employed to determine the total pore volume ($V_T$). The micropore volume ($V_{DR}$) was estimated from the Dubinin–Radushkevich equation. The mesopore volume ($V_{mes}$) was determined as the difference between the total pore volume and the micropore volume. The morphology of the bismuth sulfides was analyzed by field -emission scanning electron microscopy (FESEM, Merlin Zeiss) with an accelerating voltage of 3 kV. Transmission electron microscopy (TEM) images were recorded on TALOS F200X apparatus operating with an accelerating voltage up to 200 kV. The crystalline characteristics of the materials were studied by X-ray diffraction analyzer (XRD, Ultima IV, Rigaku) equipped with a 2 kW X-ray tube (40 kV/30 mA) using Cu K$\alpha$2 radiation ($\lambda = 1.54056 \cdot 10^{-10}$ m). The chemical composition of resultant bismuth sulfides was analyzed by X-ray photoelectron spectroscopy (XPS) using a PHI 5000 VersaProbe (ULVAC-PHI) spectrometer. The best peak fits were obtained using a Gaussian–Lorentzian (70/30) peak shape at the same FWHM for all fitted peaks.

### Electrochemical measurements

The electrodes were composed of 80 wt.% of bismuth sulfide, 10 wt.% of polyvinylidene fluoride (PVDF), and 10 wt.% of carbon black as an active electrode material, binder, and percolator, respectively. The electrodes were pressed in the form of pellets with a geometric surface area of 0.9 $cm^2$. For electrochemical measurements, three-electrode configuration was assembled in a Swagelok system. The measurements were performed in 6 mol $L^{-1}$ KOH aqueous solution using gold current collectors to avoid corrosion and to preserve comparable experimental condition. Measurements were conducted with a potentiostat–galvanostat VSP Biologic in a voltage range of $-0.8 \div -0.2$ V. The electrochemical properties of $Bi_2S_3$ samples were determined by cyclic voltammetry at a voltage scan rate of 1–100 mV $s^{-1}$ and galvanostatic charge–discharge at current densities in the range 0.2–20 A $g^{-1}$. The specific capacitance was expressed in farads per mass of active material in one electrode. The specific capacitance values ($C$/F $g^{-1}$) were calculated from the galvanostatic discharge curves and the CV curves using Eqs. (1) and (2), respectively.

$$C = \frac{\int I dt}{U m_{el}} \quad (1)$$

$$C = \frac{\int I dt}{\nu m_{el}} \quad (2)$$

where $I$ is the current (A), $U$ is the operating cell voltage (V), $t$ is the time (s), $\nu$ is the scan rate (V $s^{-1}$), and $m_{el}$ is the mass of the active material in the electrode (g). The stored energy ($E$ in Wh $kg^{-1}$) and power ($P$ in kW $kg^{-1}$) delivered by a supercapacitor based on the electrode materials were calculated using eqs. 3 and 4, respectively [5]:

$$E = \frac{CU^2}{8} \quad (3)$$

$$P = \frac{E}{t} \quad (4)$$

where $C$ is the specific capacitance of the electrode (F $g^{-1}$), $U$ is the potential window (V), and $t$ is the discharge time (s).

**Table 1** Parameters of the porous structure obtained based on $N_2$ isotherms for bismuth sulfides obtained at different temperatures

| Symbol | $S_{BET}$ $m^2$ $g^{-1}$ | $V_T$ $cm^3$ $g^{-1}$ | $V_{mes}$ $cm^3$ $g^{-1}$ | $V_{DR}$ $cm^3$ $g^{-1}$ |
|---|---|---|---|---|
| $Bi_2S_3$-0°C | 11 | 0.031 | 0.027 | 0.005 |
| $Bi_2S_3$-25°C | 16 | 0.049 | 0.040 | 0.006 |
| $Bi_2S_3$-75°C | 18 | 0.080 | 0.072 | 0.007 |

## Results and discussion

Porous structure of synthesized bismuth sulfides was determined by $N_2$ sorption at 77 K. The hysteresis loops occur in all samples regardless of synthesis temperature, confirming mesoporous nature of $Bi_2S_3$, Fig. 1a. Obtained bismuth sulfides were characterized by the poorly developed BET surface area in the range 11–18 $m^2$ $g^{-1}$. The structural parameters of obtained samples are included in Table 1. The lowest $V_T$ and $V_{mes}$ of 0.031 $cm^3$ $g^{-1}$ and 0.027 $cm^3$ $g^{-1}$, respectively, were noticed for sample synthesized at lowest temperature ($Bi_2S_3$-0°C) and characterized by the lowest surface area of 11 $m^2$ $g^{-1}$. However, within the range of temperatures from 0 to 75 °C, it is clearly seen that the porous texture of $Bi_2S_3$ is more developed when the synthesis temperature increases. The sample obtained at 75 °C is characterized by the almost twice higher total pore volume and approximately three-fold higher mesopore volume compared with $Bi_2S_3$ synthesized at 0 °C. The XRD patterns (Fig. 1b) presents very similar crystalline phase for all bismuth sulfides, which indicates that the synthesis temperature does not affect the crystalline structure. The diffraction peaks correlate with $Bi_2S_3$ orthorhombic phase. The diffraction planes were assigned in an agreement with standard diffraction pattern of $Bi_2S_3$ (JCPDS 65-2435). No impurities and $Bi_2O_3$ phase were noticed in the materials synthesized via proposed precipitation method with ammonium sulfide.

In order to receive a deeper insight into characterization of bismuth sulfides, XPS analyses were conducted. The survey spectra presented in Fig. 2a reveal signals assigned to bismuth and sulfur. The high-resolution XPS spectra of Bi 4f and S 2p were explored in order to determine the chemical state of bismuth sulfides, Fig. 2b–d. The most intensive peaks in the Bi 4f region at 163.6 and 158.3 eV are pertaining respectively to Bi $4f_{5/2}$ and Bi $4f_{7/2}$ in $Bi_2S_3$ [27]. The sample synthesized at 0 °C is characterized by the nearly symmetric shape of peaks confirming pure phase of bismuth sulfide on the surface of an analyzed material, Fig. 2b. In case of samples obtained at 25 and 75 °C, Fig. 2c and d, some distortions on shoulders of Bi $4f_{7/2}$ and Bi $4f_{5/2}$ peaks indicate heterogeneous composition of bismuth sulfide surface. Two extra peaks in the Bi 4f region at the energy binding of 164.7 and 159.4 eV can be ascribed for appearing bismuth oxide. The increase of the $Bi_2S_3$ synthesis temperature results in a formation of residual quantities of bismuth oxide on the surface, which finds the confirmation with the rise of the intensity of bismuth oxide peaks in the samples synthesized at 25 and 75 °C.

However, according to the XRD results of analogous $Bi_2S_3$, the appearing traces of the oxidized form of bismuth in the samples $Bi_2S_3$-25°C and $Bi_2S_3$-75°C are present only on the surface of materials. The magnified region of S 2p for all samples reveals the peaks of S $2p_{3/2}$ and S $2p_{1/2}$. The more intense signal recorded at 161.1 eV is ascribed to S $2p_{3/2}$ and the peak with lower intense located at energy binding of

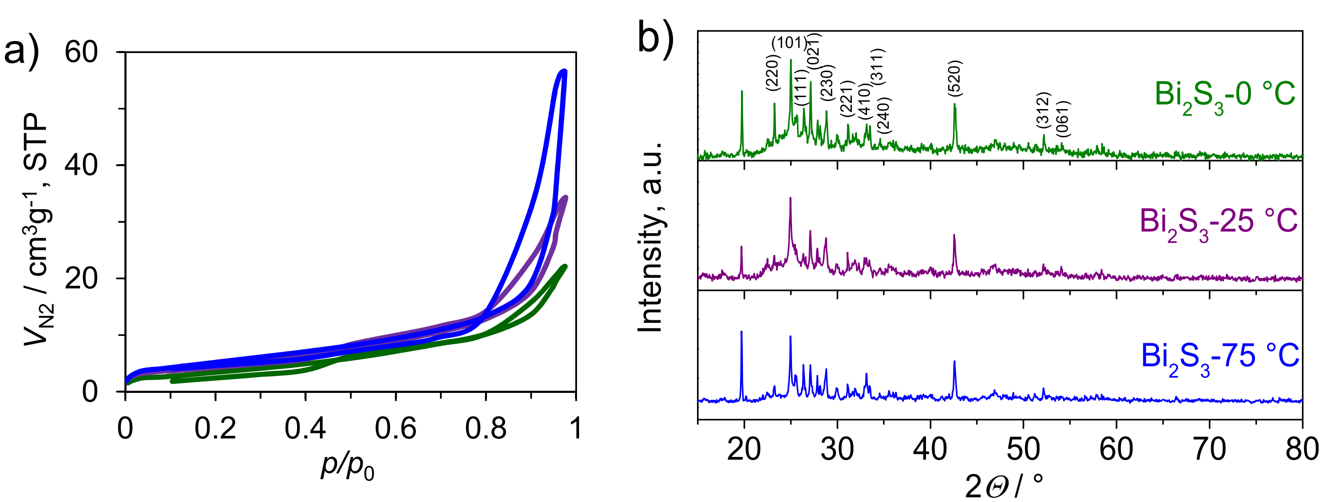


**Fig. 1** $N_2$ adsorption–desorption isotherms at 77 K (**a**) and XRD patterns of the synthesized materials (**b**)

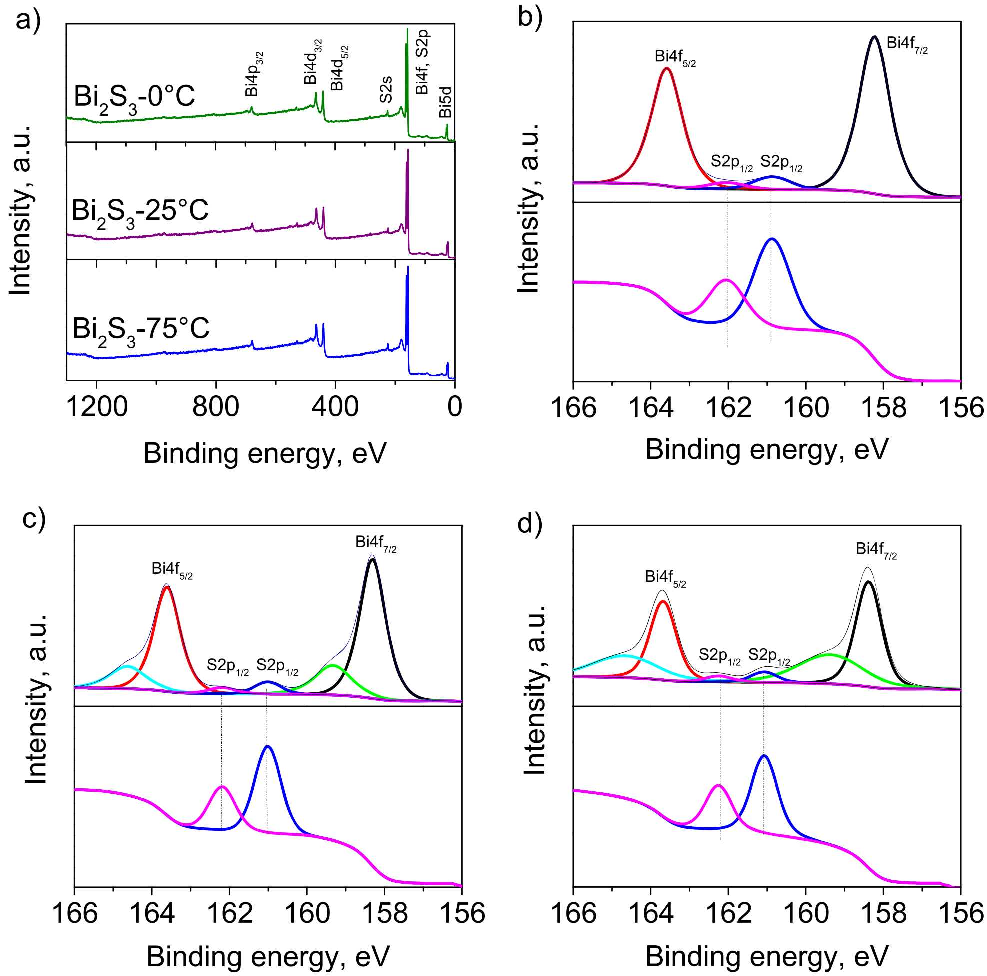


**Fig. 2** XPS survey spectra (**a**), Bi 4f and S 2p regions of $Bi_2S_3$-0°C (**b**), $Bi_2S_3$-25°C (**c**), and $Bi_2S_3$-75°C (**d**)

162.2 eV is assigned as S $2p_{1/2}$. These doublet signals confirm the primary valence state of sulfur as $S^{2-}$ [28].

The typical morphology of obtained bismuth sulfides is shown in Fig. 3. The nanorod form of $Bi_2S_3$ is recognized in all three samples regardless of synthesis temperature. Less aggregated $Bi_2S_3$ nanorods synthesized at 75 °C may influence a slight development of the specific surface area determined by $N_2$ sorption. Higher temperature leads to longer $Bi_2S_3$ nanorods, with more defects and small aggregates on the surface as the temperature increases, which can be explained by vigorous aggregation of the bismuth sulfide nanorods and accelerated collision between nucleation atoms during precipitation process [29]. The length of $Bi_2S_3$ nanorods can exceed even 5 μm, while the diameter is approximately in

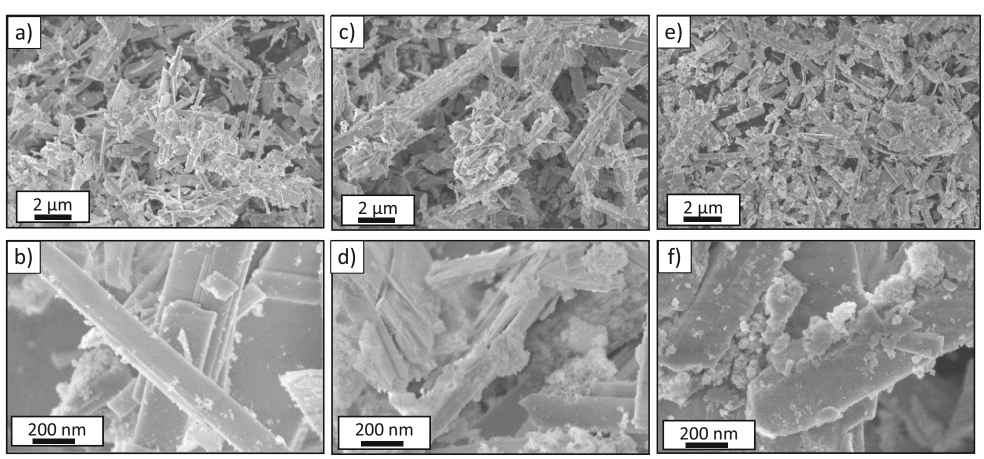


**Fig. 3** FESEM images of $Bi_2S_3$-0°C (**a**, **b**), $Bi_2S_3$-25°C (**c**, **d**) and $Bi_2S_3$-75°C (**e**, **f**)

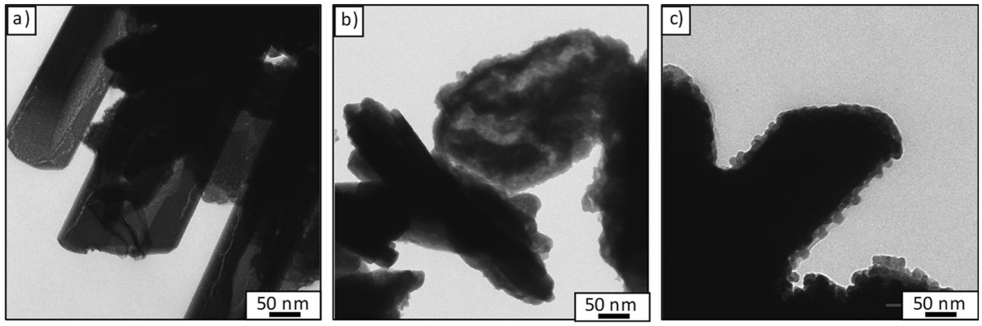


**Fig. 4** TEM images of $Bi_2S_3$-0°C (**a**), $Bi_2S_3$-25°C (**b**), and $Bi_2S_3$-75°C (**c**)

the range of 100–200 nm. The bismuth nitrate and ammonia sulfide used as a $Bi^{3+}$ and $S^{2-}$ source in the water solution promote the form of nanorods due to the inherent Bi-S chain type structure [30].

TEM images of bismuth sulfides present the nanorod-like form, which correlates with the FESEM observations (Fig. 4). Furthermore, TEM analysis revealed the presence of the secondary structures, recognized as thin films of a spherical nanoparticles on the external surface of $Bi_2S_3$ nanorods. The diameter of these nanoparticles does not exceed 20 nm, Fig. 4b. At the higher synthesis temperatures, larger amounts of these nanoparticles are distributed on the bismuth sulfide nanorods, Fig. 4c. The presence of the spherical nanostructures can provide additional electrochemically active redox sites at the electrode/electrolyte interface and increase the ratio of surface sites to the bulk sites [31].

The electrochemical performance of bismuth sulfides was investigated as working electrodes for supercapacitors operating in 6 mol $L^{-1}$ KOH aqueous electrolyte. The CV curves recorded at 2 and 50 mV $s^{-1}$ in the potential window from − 0.2 to − 0.8 V (Fig. 5a and b, respectively) reveal redox peaks, confirming the faradaic nature of bismuth sulfides rather than electric double layer. At lower scan rate, the reduction redox peaks are present at narrow potential range, indicating that $Bi_2S_3$ structure evenly undergoes a faradaic reaction, while at higher scan rate, the peaks are much wider, which can be additionally related to the overlapping reversible hydrogen adsorption–desorption processes. The anodic and cathodic peaks in the CV profiles at the potential around − 0.6 V and − 0.45 V, respectively, are attributed to the redox reaction involving $Bi_2S_3$ from the electrode material and $OH^-$ ions, as well as they originate from the change in the bismuth valence state. The redox reaction proceed with hydrogen adsorption and desorption [17, 32] according to the equation:

$$Bi_2S_3 + H_2O + e^- \leftrightarrow (H_{ads} + Bi_2S_3) + OH^- \quad (5)$$

The faradaic peak between − 0.7 and − 0.8 V represents the cathodic adsorption of hydrogen in the lamellar structure of the $Bi_2S_3$ nanorods [33]. For bismuth sulfide obtained at 75 °C, the additional cathodic peak at − 0.32 V is noticed, which is related to the hydrogen oxidation during electrochemical measurements [17]. This phenomenon suggests that during reduction, the hydrogen is stored within $Bi_2S_3$ structure via chemisorption interactions [33]. $Bi_2S_3$-75°C was characterized by the outstanding capacitance value of 739 F $g^{-1}$ at 1 mV $s^{-1}$, achieving higher value than $Bi_2S_3$-0°C and $Bi_2S_3$-25°C (527 and 552 F $g^{-1}$, respectively), Fig. 6a. When the scan rate is higher, the capacitance value decreases regardless of bismuth sulfide synthesis temperature. Lower currents registered for samples at 0 and 25 °C compared with $Bi_2S_3$ from 75 °C at higher scan rates indicates that bismuth sulfides synthesized at lower temperatures exhibit higher internal resistance values, which manifest as a significant capacitance fade. For bismuth sulfide synthesized at 75 °C, the highest capacitance value was maintained, achieving 194 F $g^{-1}$ at 100 mV $s^{-1}$, while the capacitance values of $Bi_2S_3$-0°C and $Bi_2S_3$-25°C were only 94 and 162 F $g^{-1}$, respectively. The

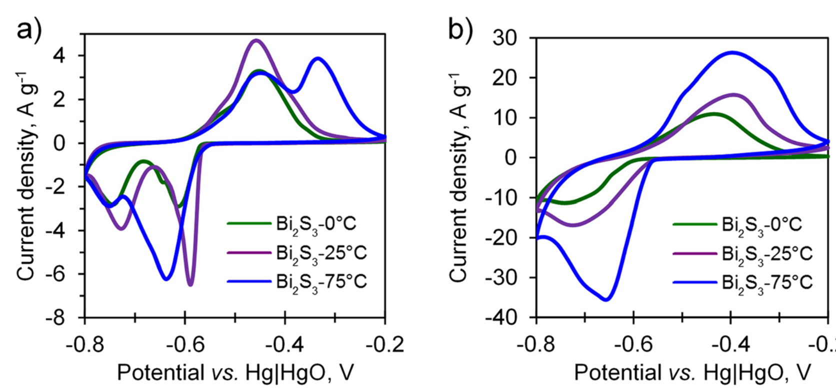


**Fig. 5** Cyclic voltammograms of bismuth sulfides synthesized at various temperatures at 2 mV $s^{-1}$ (**a**) and 50 mV $s^{-1}$ (**b**)

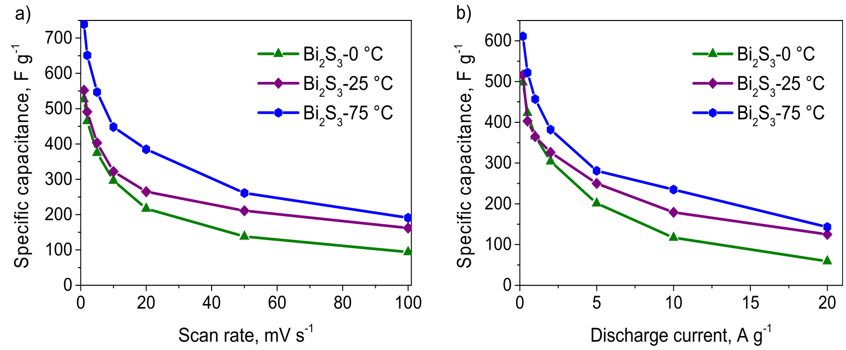


**Fig. 6** Variations of specific capacitance values of bismuth sulfides synthesized at various temperatures as a function of scan rate (**a**) and current density (**b**)

enhanced electrochemical performance of $Bi_2S_3$-75°C might be ascribed to the presence of superficial nanoparticles on the $Bi_2S_3$ nanorods, which increased the ratio of surface sites to bulk sites. These nanoparticles distribute the energy level of the redox sites over a wider potential, which broadens the faradaic peaks observed on the voltammogram As a result, there is less competition between the redox-active sites, enhancing materials pseudocapacitive performance [31]. Moreover, the highest surface area of the bismuth sulfide synthesized at the 75 °C among all samples provides the larger contact area at the electrode/electrolyte interface and facilitates ion diffusion during charging and discharging.

The galvanostatic charge and discharge curves recorded at 1 and 10 A g$^{-1}$ are depicted in Fig. 7a and b, respectively. The shape of curves suggests the faradic nature, which correlates with the CV measurements. The time of charge and discharge is noticeable longer when bismuth sulfide was synthesized at higher temperature, Fig. 7a and b. The galvanostatic discharge profiles are characterized by the two plateaus, which correspond to the peaks in the CV curves, attributed to the faradaic reactions and hydrogen adsorption–desorption processes. Moreover, the fade of the discharge plateaus at a high current density is related to the insufficient intercalation of the electrochemically active material with the electrolyte ions. The specific capacitance values of bismuth sulfides determined from galvanostatic measurements performed in 6 mol L$^{-1}$ KOH aqueous electrolyte were in the range from 498 to 611 F g$^{-1}$ at a current density of 0.2 A g$^{-1}$, and exhibit an increasing trend along with the synthesis temperature. The highest capacitance values were measured for $Bi_2S_3$-75°C in the whole current densities and scan rates range, Fig. 6. Moreover, bismuth sulfide obtained at 75 °C presented one of the highest capacitance value among other reported $Bi_2S_3$ and $Bi_2S_3$-based composites synthesized via different methods, Table 2. $Bi_2S_3$-75°C was characterized by the two and three-fold higher capacitance of 235 and 143 F g$^{-1}$ at 10 and 20 A g$^{-1}$, respectively compared to $Bi_2S_3$-0°C which was only 117 and 59 F g$^{-1}$. The best electrochemical performance of $Bi_2S_3$-75°C can be related to the most developed BET surface area and mesopore volume among all samples, Table 1. Moreover, uniform morphology of $Bi_2S_3$-75°C nanorods with a superficial spherical nanoparticles is beneficial for achieving high capacitance values and providing better electrode/electrolyte interfacial contact [24].

Electrochemical impedance spectroscopy spectra of bismuth sulfides synthesized at different temperatures are shown in Fig. 8 in the form of a Nyquist plot. A very low ESR value at 100 kHz noticed for all of the tested materials of 0.24, 0.29, and 0.10 Ω for $Bi_2S_3$ obtained at 0 °C, 25 °C, and 75 °C, respectively, can be ascribed to their good conductive properties. A semicircle in the high-frequency region is observed for all samples, indicating fast ion kinetics due to the crystalline structure. The most inclined line towards – Z axis for $Bi_2S_3$-75°C indicates the lowest Warburg resistance among all samples, which is related to the ability of the electrolyte ions to penetrate into pores of the electrode material. The more horizontal lines of $Bi_2S_3$ from 0 and 25°C suggest difficulties of ion transport into the bulk material [37].

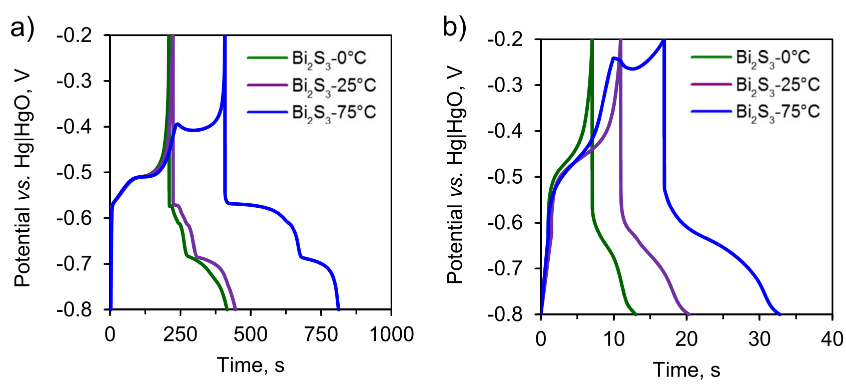


**Fig. 7** Charge-discharge profiles of bismuth sulfides recorded at 1 A g$^{-1}$ (**a**) and 10 A g$^{-1}$ (**b**)

**Table 2** Comparison of electrochemical properties of $Bi_2S_3$-based materials synthesized under different conditions

| Sample name | Synthesis method | Morphology | Electrolyte | Specific capacitance | Ref. |
|---|---|---|---|---|---|
| $Bi_2S_3$ modified with Co $(OH)_2$ | Hydrothermal method | Nanorods | 0.5 M $Na_2SO_4$ | 113.3 mF cm$^{-2}$ at 0.2 mA cm$^{-2}$ | [17] |
| $Bi_2S_3$ | Hydrothermal method | Nanoflowers | 6 M KOH | 233 F g$^{-1}$ at 1 A g$^{-1}$ | [23] |
| $Bi_2S_3$-rGO | Precipitation in reflux at 200 °C | Nanorods | 2 M KOH | 290 F g$^{-1}$ at 1 A g$^{-1}$ | [24] |
| $Bi_2S_3$ | Solvothermal method | Nanorods | 1 M $Na_2SO_4$ | 270 F g$^{-1}$ at 1 A g$^{-1}$ | [26] |
| $Bi_2S_3$-rGO | Hydrothermal method | Nanorods | 2 M KOH | 396 F g$^{-1}$ at 1 A g$^{-1}$ | [28] |
| $Bi_2S_3$ | Hydrothermal method | Nanoflowers | 5 M KOH | 94.3 F cm$^{-2}$ at 2 mA cm$^{-2}$ | [34] |
| $Bi_2S_3$ | SILAR method | Thin film nanoparticles | 1 M $Na_2SO_4$ | 289 F g$^{-1}$ at 5 m Vs$^{-1}$ | [35] |
| $Bi_2S_3$-rGO | Hydrothermal method | Nanoparticles | 1 M $Na_2SO_4$ | 292 F g$^{-1}$ at 1 A g$^{-1}$ | [36] |
| $Bi_2S_3$-75°C | Chemical precipitation | Nanorods | 6 M KOH | 457 F g$^{-1}$ at 1 A g$^{-1}$ | This work |

The relationship between power and energy densities in the form of Ragone plot is presented in Fig. S1. The achieved energy densities of the synthesized bismuth sulfides are in the range from 7.6 to 6.2 Wh kg$^{-1}$ at power densities from 24 to 32 W kg$^{-1}$. In comparison, commercially available supercapacitors based on organic electrolytes deliver around 2–6 Wh kg$^{-1}$ of energy [38]. At higher power density above 3 kW kg$^{-1}$, a significant decrease of the stored energy is observed for the $Bi_2S_3$ from lower temperatures due to the capacitance fade. The highest energy density is maintained by $Bi_2S_3$-75°C, presenting 2 Wh kg$^{-1}$ at a power density of 2.9 kW kg$^{-1}$ in an aqueous electrolyte.

For further investigation, the cycling performance of the synthesized bismuth sulfides by the galvanostatic charge-discharge tests at a current density of 1 A g$^{-1}$ has been performed (Fig. 9). The capacitance fade of the electrode material observed under cycling can be ascribed to mechanical stress due to the reversible insertion/de-insertion of electrolyte ions into the bulk material [28]. Moreover, the spherical nanoparticles at the surface of the nanorods may aggregate during cycling, leading to the decrease of the amount of active sites available for the redox reactions. Bismuth sulfides obtained at 0 and 25 °C revealed comparable capacitive performance after cycling, presenting 128 and 141 F g$^{-1}$, respectively. Among all samples, the $Bi_2S_3$ obtained at 75 °C maintained the highest initial capacitance value after 1000 charge–discharge cycles, achieving 236 F g$^{-1}$. The porous structure and unique morphology of $Bi_2S_3$-75 °C in comparison with bismuth sulfides synthesized at 0 and 25 °C resulted in an improved electrochemical behavior, both in terms of the capacitive performance and cyclic stability.

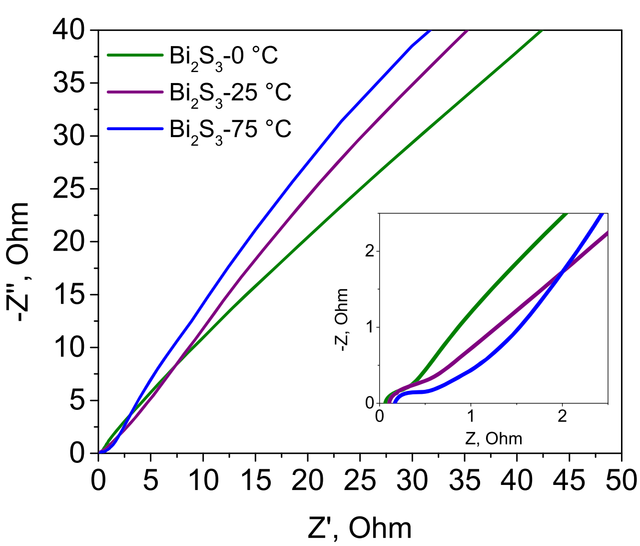


**Fig. 8** Nyquist plots of bismuth sulfides obtained at different temperatures with inset representing the high-frequency region

## Conclusions

Bismuth sulfides in the form of nanorods were successfully synthesized via facile chemical precipitation method. Despite the temperature range, all materials present similar crystalline

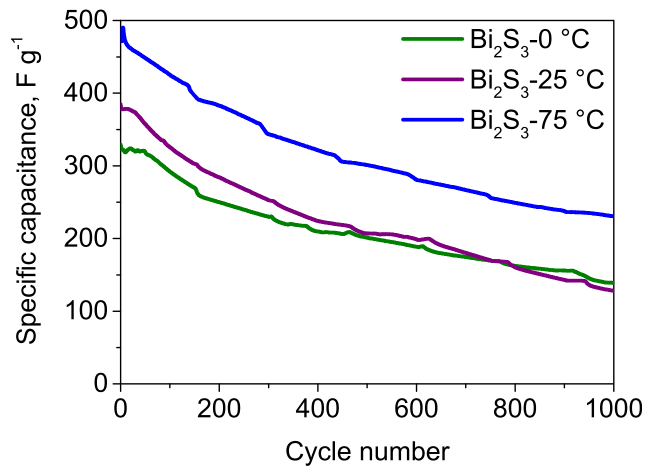


**Fig. 9** Cyclic performances of $Bi_2S_3$ synthesized at different temperatures at a current density of 1 A g$^{-1}$

structure. $N_2$ sorption analysis shows the largest mesopore volume for $Bi_2S_3$ prepared at 75 °C. Although the bismuth sulfides present low specific surface areas, neglecting the contribution of electrical double-layer capacitance, they exhibit high specific capacitance values from 527 to 739 F $g^{-1}$ at a scan rate of 1 mV $s^{-1}$ in a three-electrode cell, which confirm their faradaic behavior. Among all synthesized sulfides, $Bi_2S_3$-75°C was characterized by the best electrochemical performance, achieving capacitance value of 457 F $g^{-1}$ at 1 A $g^{-1}$ and a three-fold higher capacitance at 20 A $g^{-1}$ in comparison to bismuth sulfides obtained at lower temperatures. The outstanding electrochemical performance observed for $Bi_2S_3$ synthesized at 75 °C is a result of uniform, nanorod-like morphology with a spherical nanoparticle thin film, which increased the ratio of the electrochemically active redox sites. Moreover, $Bi_2S_3$-75°C exhibited the most developed porous structure among all synthesized bismuth sulfides, facilitating the electrolyte ions movement at the electrode/electrolyte interface.

**Funding information** The research leading to above results has received funding from the National Science Centre (Poland) under the grant agreement 2016/21/D/ST5/01642.





## References

1. Jang Y, Jo J, Choi Y-M, Kim I, Lee S-H, Kim D, Yoon SM (2013) Activated carbon nanocomposite electrodes for high performance supercapacitors. Electrochim Acta 102:240–245
2. Śliwak A, Grzyb B, Ćwikła J, Gryglewicz G (2013) Influence of wet oxidation of herringbone carbon nanofibers on the pseudocapacitance effect. Carbon 64:324–333
3. Moyseowicz A, Śliwak A, Miniach E, Gryglewicz G (2016) Influence of structural and textural parameters of carbon nanofibers on their capacitive behavior. J Mater Sci 51(7):3431–3439
4. Pandolfo AG, Hollenkamp AF (2006) Carbon properties and their role in supercapacitors. J Power Sources 157(1):11–27
5. Moyseowicz A, Gryglewicz G (2019) Hydrothermal-assisted synthesis of a porous polyaniline/reduced graphene oxide composite as a high-performance electrode material for supercapacitors. Composites B: Engineering 159:4–12
6. Śliwak A, Grzyb B, Diez N, Gryglewicz G (2017) Nitrogen-doped reduced graphene oxide as electrode material for high rate supercapacitors. Appl Surf Sci 399:265–271
7. Gao F, Qu J, Zhao Z, Wang Z, Qiu J (2016) Nitrogen-doped activated carbon derived from prawn shells for high-performance supercapacitors. Electrochim Acta 190:1134–1141
8. Gryglewicz G, Śliwak A, Beguin F (2013) Carbon nanofibers grafted on activated carbon as an electrode in high-power supercapacitors. ChemSusChem 6(8):1516–1522
9. Zhang X, Yu P, Zhang H, Zhang D, Sun X, Ma Y (2013) Rapid hydrothermal synthesis of hierarchical nanostructures assembled from ultrathin birnessite-type $MnO_2$ nanosheets for supercapacitor applications. Electrochim Acta 89:523–529
10. Śliwak A, Gryglewicz G (2014) High-voltage asymmetric supercapacitors based on carbon and manganese oxide/oxidized carbon nanofiber composite electrodes. Energy Technol 2(9-10): 819–824
11. Miniach E, Śliwak A, Moyseowicz A, Fernández-Garcia L, González Z, Granda M, Menendez R, Gryglewicz G (2017) $MnO_2$/thermally reduced graphene oxide composites for high-voltage asymmetric supercapacitors. Electrochim Acta 240:53–62
12. Zhang Z, Huang Z, Ren L, Shen Y, Qi X, Zhong J (2014) One-pot synthesis of hierarchically nanostructured $Ni_3S_2$ dendrites as active materials for supercapacitors. Electrochim Acta 149:316–323
13. Wei W, Mi L, Gao Y, Zheng Z, Chen W, Guan X (2014) Partial ion-exchange of nickel-sulfide-derived electrodes for high performance supercapacitors. Chem Mater 26(11):3418–3426
14. Huang K-J, Zhang JZ, Shi GW, Liu Y-M (2014) One-step hydrothermal synthesis of two-dimensional cobalt sulfide for high-performance supercapacitors. Mater Lett 131:45–48
15. Chen W, Xia Z, Alshareef HN (2014) One-step electrodeposited nickel cobalt sulfide nanosheet arrays for high-performance asymmetric supercapacitors. ACS Nano 8(9):9531–9541
16. Tie J, Han J, Diao G, Liu J, Xie Z, Cheng G, Sun M, Yu L (2018) Controllable synthesis of hierarchical nickel cobalt sulfide with enhanced electrochemical activity. Appl Surf Sci 435:187–194
17. Yang H, Xie J, Li CM (2014) $Bi_2S_3$ nanorods modified with $Co(OH)_2$ ultrathin nanosheets to significantly improve its pseudocapacitance for high specific capacitance. RSC Adv 4(89): 48666–48670
18. Durga IK, Rao SS, Reddy AE, Gopi CVVM, Kim H-J (2018) Achieving copper sulfide leaf like nanostructure electrode for high performance supercapacitor and quantum-dot sensitized solar cells. Appl Surf Sci 435:666–675
19. Peng XS, Meng GW, Zhang J, Zhao LX, Wang XF, Wang YW, Zhang LD (2001) Electrochemical fabrication of ordered $Bi_2S_3$ nanowire arrays. J Phys D Appl Phys 34(22):3224–3228
20. Sheng Q, Shen Y, Wu Q, Zheng J (2016) Direct electrochemistry and electrocatalysis of cytochrome *c* based on dandelion-like $Bi_2S_3$ nanoflowers. J Solid State Electrochem 20(12):3315–3322
21. Liao XH, Wang H, Zhu JJ, H, Chen H-Y (2001) Preparation of $Bi_2S_3$ nanorods by microwave irradiation. Mater Res Bull 36: 2339–2346, 13-14
22. Chen Y, Kou H, Jiang J, Su Y (2003) Morphologies of nanostructured bismuth sulfide prepared by different synthesis routes. Mater Chem Phys 82(1):1–4
23. Liu KL, Chen F, Liu Y, Li D, Shi WD (2017) Synthesis of hierarchical $Bi_2S_3$ nanoflowers via a topotatic transformation from hierarchical $Bi_2WO_6$ nanoflowers and their supercapacitor performance. CrystEngComm 19(3):570–575
24. Vadivel S, Naveen AN, Kamalakannan VP, Cao P, Balasubramanian N (2015) Facile large scale synthesis of $Bi_2S_3$ nano rods-graphene composite for photocatalytic photoelectrochemical and supercapacitor application. Appl Surf Sci 351:635–645
25. Shinde DV, Patil SA, Cho K, Ahn DY, Shrestha NK, Mane RS, Lee JK, Han S-H (2017) Revisiting metal sulfide semiconductors: a solution-based general protocol for thin film formation, hall effect measurement, and application prospects. Adv Funct Mater 25: 5739–5747

26. Liang K, Wang C, Xu X, Leng J, Ma H (2017) Capacitive and photocatalytic performance of $Bi_2S_3$ nanostructures synthesized by solvothermal method. Phys Lett A 381(6):652–657
27. He H, Berglund SP, Xiao P, Chemelewski WD, Zhang Y, Mullins ZB (2013) Nanostructures $Bi_2S_3/WO_3$ heterojunction films exhibiting enhanced photoelectrochemical performance. J Mater Chem A 1(41):12826–12834
28. Nie G, Lu X, Lei J, Yang L, Wang C (2015) Facile and controlled synthesis of bismuth sulfide nanorods-reduced graphene oxide composites with enhanced supercapacitor performance. Electrochim Acta 154:24–30
29. Shaziman S, Ismail@rosdi AS, Mamat MH, Zoolfakar AS (2015) Influence of growth time and temperature on the morphology of ZnO nanorods via hydrothermal. IOP Conf. Series: Mater Sci Eng 99:012016
30. Tian L, Tan HY, Vittal JJ (2008) Morphology-controlled synthesis of $Bi_2S_3$ nanomaterials via single- and multiple-source approaches. Cryst Growth Des 8(2):734–738
31. Eftekhari A, Mohamedi M (2017) Tailoring pseudocapacitive materials from a mechanistic perspective. Mater Today Ener 6:211–229
32. Jin R, Li G, Zhang Z, Yang L-X, Chen G (2015) Carbon coated flower like $Bi_2S_3$ grown on nickel foam as binder-free electrodes for electrochemical hydrogen and Li-ion storage capacities. Electrochim Acta 173:458–464
33. Zhang B, Ye X, Hou W, Zhao Y, Xie Y (2006) Biomolecule-assisted synthesis and electrochemical hydrogen storage of $Bi_2S_3$ flowerlike patterns with well-aligned nanorods. J Phys Chem B 110(18):8978–8985
34. Ma L, Zhao Q, Zhang Q, Ding M, Huang J, Liu X, Liu Y, Wu X, Xu X (2014) Controlled assembly of $Bi_2S_3$ architectures as Schottky diode, supercapacitor electrodes and highly efficient photocataysts. RSC Adv 4(78):41636–41641
35. Raut SS, Dhobale JA, Sankapal BR (2017) SILAR deposited $Bi_2S_3$ thin film towards electrochemical supercapacitor. Phys E Low Dimens Syst Nanostruct 87:209–212
36. Lu H, Guo Q, Zan F, Xia H (2017) $Bi_2S_3$ nanoparticles anchored on graphene nanosheets with superior electrochemical performance for supercapacitors. Mater Res Bull 96:471–477
37. He W, Liang Z, Ji K, Sun Q, Zhai T, Xu X (2018) Hierarchical Ni–Co–S@Ni–W–O core-shell nanosheet arrays on nickel foam for high-performance asymmetric supercapacitors. Nano Res 11(3):1415–1425
38. Yassine M, Fabris D (2017) Performance of commercially available supercapacitors. Energies 10(9):1340